HHS Public Access

Author manuscript

J Comput Chem. Author manuscript; available in PMC 2016 September 30.

Published in final edited form as:

J Comput Chem. 2015 September 30; 36(25): 1859–1873. doi:10.1002/jcc.24011.

Comparison of Radii Sets, Entropy, QM Methods, and Sampling on MM-PBSA, MM-GBSA, and QM/MM-GBSA Ligand Binding Energies of *F. tularensis* Enoyl-ACP Reductase (FabI)

Pin-Chih Su[1], **Cheng-Chieh Tsai**[1], **Shahila Mehboob**[1], **Kirk E. Hevener**[1,2], and **Michael E. Johnson**[1]

[1] Center for Pharmaceutical Biotechnology, College of Pharmacy, University of Illinois at Chicago, Chicago, IL, U.S.A., 60607

Abstract

To validate a method for predicting the binding affinities of FabI inhibitors, three implicit solvent methods, MM-PBSA, MM-GBSA and QM/MM GBSA were carefully compared using sixteen benzimidazole inhibitors in complex with *F. tularensis* FabI. The data suggests that the prediction results are sensitive to radii sets, GB methods, QM Hamiltonians, sampling protocols, and simulation length, if only one simulation trajectory is used for each ligand. In this case, QM/MM-GBSA using 6 ns MD simulation trajectories together with GB^{neck2}, PM3, and the mbondi2 radii set, generate the closest agreement with experimental values (r^2= 0.88). However, if the three implicit solvent methods are averaged from six 1 ns MD simulations for each ligand (called "multiple independent sampling"), the prediction results are relatively insensitive to all the tested parameters. Moreover, MM/GBSA together with GB^{HCT} and mbondi, using 600 frames extracted evenly from six 0.25 ns MD simulations, can also provide accurate prediction to experimental values (r^2 = 0.84). Therefore, the multiple independent sampling method can be more efficient than a single, long simulation method. Since future scaffold expansions may significantly change the benzimidazole's physiochemical properties (charges, etc.) and possibly binding modes, which may affect the sensitivities of various parameters, the relatively insensitive "multiple independent sampling method" may avoid the need of an entirely new validation study. Moreover, due to large fluctuating entropy values, (QM/)MM-P(G)BSA were limited to inhibitors' relative affinity prediction, but not the absolute affinity. The developed protocol will support an ongoing benzimidazole lead optimization program.

Keywords

radii sets; enoyl acyl reductase (FabI); implicit solvent models; molecular dynamics; quantum mechanics/molecular mechanics (QM-MM)

Correspondence to: Kirk E. Hevener (khevener@pharmacy.isu.edu) & Michael E. Johnson (mjohnson@uic.edu).

[2]Current Address: Department of Biomedical and Pharmaceutical Sciences, College of Pharmacy, Idaho State University, Meridian, ID, U.S.A., 83642

Additional Supporting Information may be found in the online version of this article.

Introduction

Tularemia, a deadly zoonotic infection caused by the Gram-negative pathogen *Francisella tularensis*, is a viable bioweapon due to its ease of cultivation and aerosolization as well as its low infectious dose.[1] Although treatments for tularemia are available, including aminoglycoside antibiotics, streptomycin, ciprofloxacin and tetracycline, a widespread outbreak of this disease may still be unmanageable due to their requirement for intravenous use (aminoglycosides, streptomycin) or contraindication for use in pregnant women and children (ciprofloxacin, tetracyclines).[2] There is, therefore, a strong interest within the antibacterial research community in the identification and development of novel agents with improved physicochemical properties and activity against *F. tularensis*.

The bacterial fatty acid synthesis (FAS-II) metabolic pathway, which is responsible for the synthesis of fatty acid components of bacterial lipid membranes and energy stores, is an attractive antibacterial target. Distinct from its mammalian FAS-I counterpart, which consists of a single, large, multifunctional enzyme with low similarity, the bacterial FAS-II pathway is composed of separate enzyme steps with low similarity to FAS-I. The differences between FAS-I and FAS-II allow for the selective targeting of FAS-II enzymes, while minimizing disruption to the mammalian FAS-I pathway, a significant advantage in antibacterial drug design. The enoyl-[acyl-carrier-protein] reductase enzyme, FabI, catalyzes a key, rate-limiting reduction step in bacterial fatty acid synthesis and is considered to be one of the more attractive enzyme targets in the FAS-II pathway.

We have previously reported the identification of a series of benzimidazole compounds with FabI inhibitory activity as well as *F. tularensis* antibacterial activity using a novel shape/electrostatic virtual screening campaign.[3] In addition to activity against *F. tularensis*, the benzimidazoles showed strong antibacterial activity against other Gram-positive and Gram-negative pathogens. Further, structural studies performed in-house revealed that the benzimidazole compounds bound to the FabI active site in a conformation that was unique from other known FabI inhibitors, including triclosan, a marketed antiseptic (**Figure 1**).[4-6] This suggested the possibility that the benzimidazole compounds might have utility against *F. tularensis* strains bearing resistance to other FabI targeting antibacterials, including triclosan. Additional metabolic and toxicity studies showed that the benzimidazole scaffold possessed moderate metabolic stability and low cell toxicity.[7] Taken together, the biological, microbiological, and pharmacokinetic data collected to date justify the further biochemical optimization of the benzimidazole compounds as a lead series for treatment of *F. tularensis* and possibly other bacterial infection.

The goal of the studies presented here was the development of a computational method that could predict the FabI binding affinity of benzimidazole compounds that were being proposed for synthesis and testing. The rationale was that a reliable computational affinity prediction protocol could allow for a more efficient and rapid lead optimization process by identifying compounds, prior to costly synthesis and testing, that were predicted to have high binding affinity to the FabI target. In previous work, we extensively studied various molecular docking and scoring algorithms for use in predicting relative FabI affinity, however these methods generally failed to accurately rank benzimidazole compounds by

binding affinity in validation trials.[3] This was likely due to insufficient conformational sampling of a flexible loop near the substrate/ligand binding site as well as inaccuracies in the scoring functions utilized. Herein, we report our studies of more advanced computational methods for predicting the binding affinity of the benzimidazole compounds to *F. tularensis* FabI, including MM-PBSA, MM-GBSA, and QM/MM-GBSA. Previous work has shown that the MM/P(G)BSA methods can accurately predict relative binding free energies of similar compounds using enhanced energy sampling from simulations combined with solvation energy estimations using implicit methods.[8] We chose to explore these implicit solvent methods over more advanced explicit solvent methods, such as free energy perturbation and thermodynamic integration, as the higher computational expense of the latter methods would adversely impact the throughput of our planned lead optimization studies.[9]

Although MM-P(G)BSA methods have been used successfully in both virtual screening[10,11] and lead optimization programs[12-17], it has been shown that the results are sensitive to atomic charges, simulation length, entropy calculations, and sampling protocols which can lead to dramatic differences in affinity predictions using the same study system.[18-21] Studies have also suggested that prediction results of MM-GBSA methods might be influenced by radii settings.[22-29] Additionally, a recent study suggested that multiple independent simulations in MM-GBSA offered improved statistically converged results over one long MD simulation.[30] Thus, it was also of interest to see if multiple independent samplings offer a better agreement between experimental and calculated binding free energy than a single, long MD simulation for the studied system. Lastly, the recently developed hybrid QM/MM-GBSA method[31-34] has yet to be extensively compared with MM-GBSA methods with respect to the factors just mentioned.[35]

Within this context and our ultimate goal of developing the most suitable method to support our lead optimization program, we have performed a series of comparative trials using the *F. tularensis* FabI (*Ft*FabI) structure and sixteen benzimidazole compounds with known affinity from experimental studies and several experimentally confirmed binding conformations. These studies were specifically designed to answer the following questions: **(1)** What is the best combination of radii settings, QM Hamiltonians, implicit solvent methods, and simulation length for the studied system? **(2)** If entropy calculations are included, will they improve the prediction results? **(3)** Can multiple independent samplings improve the prediction of binding free energy over the use of one long simulation for the methods studied? And ultimately, **(4)** Which optimized method offers the best predictive power in terms of the absolute and relative binding affinity for our study system?

Methods

Complex Preparation

The binding conformation of FtFabI-benzimidazole complexes were taken from co-crystal structures solved in-house (PDB codes: 3UIC, 4J3F, 4J4T).[4,6] RESP atomic partial charges were assigned to benzimidazole ligands and the cofactor, NADH, with geometry optimization and the electrostatic potential calculations performed using HF/6-31G* and Gaussian 09[36] in the R.E.D. server.[37-39] The AMBER FF12SB force field and the general

AMBER force field (GAFF)[40] parameters were assigned to the protein and the ligand using *antechamber* in AMBER v12.[41] A 10Å TIP3P water molecule octahedron box was set to solvate the complex system along with Na^+ and Cl^- counter-ions to neutralize the system.

Experimental Enzymatic Activity

The FabI enzyme reduces butenyl-CoA to butyryl-CoA utilizing the cofactor NADH. Enzyme activity was monitored by following the rate of decrease in fluorescence of NADH at 450 nm (excitation wavelength 340 nm). Detailed methods for the determination of the IC_{50} and K_i values of the benzimidazole compounds against FtFabI have been previously described.[3,4,6] The compounds used in this study are shown in **Supplementary Table 1**, along withexperimental inhibition data. The experimental free energies of binding (ΔG_{bind}) were calculated from K_i using Equation 1, where R is the ideal gas constant (1.9872×10^{-3} kcal K^{-1} mol^{-1}) and T is the room temperature (300K).

$$\Delta Gbind = RT \quad lnKi \quad (1)$$

Molecular Dynamics (MD) Simulations

The systems were first minimized using 5000 steps of steepest descent minimization using the Particle Mesh Ewald (PME) potential function. After minimization, the systems were heated from 0K to 300K over 50 picoseconds (ps) using the NVT ensemble with a 10 kcal/mol-Å weak restraint on the enzyme, cofactor and ligands. Following this, the systems were equilibrated over 50 ps at constant pressure (1 bar) and temperature (300K) using NPT equilibration. Next, a 6 nanosecond (ns) NPT production run was performed at 300 K and 1 bar. The following settings were activated in all of the equilibration and production run MD simulations: Langevin dynamics for temperature scaling, 2 ps as the pressure relaxation time, 8 Å electrostatic interactions cut off, the SHAKE bond length constraints of hydrogen atoms, and 1 fs time step. In the production runs, the MD simulation trajectories were saved every 2.5 ps for subsequent (QM/)MM-P(G)BSA analyses. The *pmemd.MPI* program in AMBER12 was used for all of the above minimizations and simulations.

MM-PBSA

The MM-PBSA calculations were performed using *MMPBSA.py* in AMBERTools13.[42] When the PARSE, bondi, mbondi, and mbondi2 sets were applied, the MM-PBSA surface tension (α) and the non-polar free energy correction term (β) were set to 0.00542 kcal/mol-$Å^2$ and 0.92, respectively, following the recommendation of the original PARSE radii study[43] and the AMBER user manuals.[41] An exterior dielectric constant of 80 and solute dielectric constant of 1 were used. 2,400 snapshots were taken evenly from the MD simulations trajectory from 0 to 6 ns in the MM-PBSA calculations.

MM-GBSA and QM/MM-GBSA

The (QM)/MM-GBSA calculations were performed using *MMPBSA.py* in AMBERTools13. We investigated several GB models in this study, including the pairwise model developed by Hawkins et al. (GB^{HCT}),[23] the model developed by Onufriev et al. (GB^{OBC}),[24] the optimized version of GB^{OBC} (GB^{OBC2}),[25] the model developed by Mogan et al. to solve the

so-called "bottle-neck" issue (GB^{Neck}),[26] and the optimized version of GB^{Neck} (GB^{Neck2}).[27] Additional details are provided in **Supplementary Table 2**. The bondi, mbondi, and mbondi2 radii sets were prepared using the *antechamber* program in AMBER12. In AMBERTools13, the default setting of MM-GBSA surface tension (α = 0.0072 kcal / mol $Å^2$) and the non-polar free energy correction term ($\beta = 0$) were applied. In the QM/MM-GBSA, the benzimidazole ligand was treated as the QM region using the AM1, PM3 and PM6 semi-empirical Hamiltonian theories. The QM charge of the ligand was set to zero because none of the ligands in this study are expected to carry a formal charge at physiological pH. The remaining QM/MM-GBSA settings are identical to the above MM-GBSA section.

Entropy

The entropy calculations were performed using Normal Mode Analysis (NMA) in the *MMPBSA.py* program in AMBERTools13.[44] The following were the settings for the entropy calculations: The distance-dependent dielectric constant was set to 1.0, and the energy gradient of minimization was 0.001 with 10,000 minimization cycles per snapshot. Due to limited computational resources, we used only 48 frames, which were evenly extracted from 0 to 6 ns of the MD trajectories for entropy calculations.

Multiple Independent MD Simulations

The multiple independent MD simulations were prepared using the same settings and starting structures described above, with the exception that the random starting velocities were applied by turning on the pseudo-random starting velocity generator (the "ig" flag in AMBER12). In order to compare the differences between these and single 6 ns MD simulations, the MD simulations were separated into six, 1 ns components. For the MM-PBSA and (QM/)MM-GBSA, 400 snapshots were taken evenly from each of the six, 1-ns MD simulation trajectories from 0 to 1 ns. Other settings for the MM-PBSA, MM-GBSA, and QM/MM-GBSA calculations for multiple MD simulations were as described above.

Results and Discussion

The Effect of MD Simulation Length on MM-PBSA

The coefficient of determination between experimental and predicted binding free energies using different MD trajectory lengths and radii settings in MM-PBSA calculations are summarized in **Table 1**. The MM-PBSA calculations based on the 0.25 to 2.00 ns MD trajectories were satisfactory (r^2>0.70) in all bondi, mbondi, mbondi2, and PARSE radii sets. However, using data from MD trajectories equal to or longer than 2 ns for the MM-PBSA calculations seemed to lower the accuracy of prediction in all four radii settings. To further analyze the nature of the decrease in predictive power with longer MD simulation times, we first checked the MM-PBSA energy terms plot of FtFabI- GRL-0056 **(Figure 2)** and the rest of fifteen ligands **(Supplementary Figure 1)**. The yellow line was the instantaneous enthalpy of binding (ΔG_{bind}) and it can be readily seen that all the ΔG_{bind} in the sixteen ligands using all the radii settings were readily converged. Therefore, it is likely that the decrease in predictive power along the MD simulation time frames is due to an

amplification of force field errors along the MD simulation time frames, instead of non-converged energy in the system, as reported in the previous study.[21]

The Effect of Radii Sets on MM-PBSA

The impact of four different radii sets (bondi, mbondi, mbondi2, and PARSE) are also summarized in **Table 1**. It can be clearly seen that bondi and mbondi2 gave almost identical predictive power since bondi and mbondi2 were optimized via similar theoretical frame works.[27] Interestingly, the difference in predictive power between mbondi versus bondi and mbondi2 was also quite small. Considering the potential errors of the experimental binding free energy, these differences show little significance. Among the four radii sets, the PARSE radii offered the poorest correlation with experimental values using MD trajectories shorter than 2 ns (r^2= 0.62 - 0.77). A possible explanation is that the GB radii sets (bondi, mbondi, and mbondi2) are more extensively parameterized in various atom types for each chemical element while the PARSE radii set has only one atom type for each chemical element, as discussed in previous studies. [21, 43] Finally, in **Supplementary Table 3**, one can clearly see that the three Born radii sets always generated smaller solvation energy terms ($\Delta G_{solvation}$) and correspondingly more negative binding enthalpy values (ΔH_{bind}) than the PARSE radii sets. A similar effect was noted in a previous study.[21] A possible reason is that the three Born radii sets contain larger radii and larger corresponding dielectric boundaries than the PARSE radii set and therefore result in higher solvation energy terms when applying the three bondi radii sets. [21,23-26,43,45]

The Effect of MD Simulation Length on MM-GBSA

The coefficient of determination of experimental and predicted binding free energies for different MD trajectory lengths and radii sets in MM-GBSA calculations are summarized in **Table 2**. The predictive power of the MM-GBSA method with longer simulations decreased in a manner similar to the MM-PBSA predictions. For all three radii sets, the MM-GBSA predictions based on MD trajectories less than or equal to 1 ns were in the satisfactory range ($R^2 > 0.7$), while the predictive power dropped significantly when using MD trajectories larger than 1 ns. As above, the decrease in predictive power may be due to the amplification of force field errors. [21]

Interestingly, although the predictive power of GB^{Neck2} also decreased with longer MD simulations, the extent of the decrease was less than for the other four GB methods (R^2 = 0.6 at 1 ns and R^2 = 0.51 at 6 ns). This might suggest that GB^{Neck2} provided better agreement to the experimental values in terms of solvation energy and therefore offset the degree of predictive power diminishment. This will be discussed in more detail below in the QM/MM-GBSA section.

The Effect of Radii Sets on MM-GBSA

It is known that MM-GBSA is more sensitive to various radii sets than MM-PBSA, and earlier studies have suggested the optimal radii set (s) for each GB method (summarized in **Supplementary Table 2**).[23-26,45] The mbondi radii set was a non-recommended radii setting for GB^{OBC}. However, as shown in **Table 2**, in our studies the three different radii sets in GB^{OBC} resulted in only minor differences. Thus, for this system, considering the

potential errors in experimental free energy of binding, the differences between the predictive powers of the three radii sets for the GB^{OBC} method can be safely ignored. In GB^{OBC}, GB^{OBC2}, GB^{Neck} and GB^{Neck2}, it is not surprising that the suggested radii sets, bondi and mbondi2, yielded nearly identical prediction results because mbondi2 is a modification of and very similar to bondi **(Table 2)**.[45] We did not include the mbondi set in the GB^{Neck} and GB^{Neck2} calculations, since earlier studies did not recommend the mbondi setting in the GB^{Neck} and GB^{Neck2} methods, and *MMPBSA.py* in the AMBERTools13 suite did not allow the mbondi radii set in the default GB^{Neck} and GB^{Neck2} methods. Additionally, in GB^{OBC2}, our data in **Table 2** did suggest that the predicted binding free energy calculated by bondi and mbondi2 radii sets correlated better with the experimental binding free energy than the unfavorable mbondi settings.

The three radii sets and their corresponding effects on the solvation energy terms are summarized in **Supplementary Figure 2 & Supplementary Table 4**. When MM-GBSA calculations were performed under similar conditions (inhibitor, number of MD frames, GB method, and charges) using the different radii sets, the only energy terms showing significant changes are the polar energy term (ΔG_{GB}), the total solvation energy term ($\Delta G_{solvation}$), and the total free energy of binding, ΔG_{bind} (the red, blue, yellow lines on top of each figure in **Supplementary Figure 2** respectively and Equation 2). This is due to the fact that radii settings only affect ΔG_{GB} and $\Delta G_{solvation}$. From the ΔG_{GB} energy curves in **Supplementary Figure 2**, bondi and mbondi2 result in nearly identical solvation energy values while mbondi consistently offered more positive ΔG_{GB} values than bondi and mbondi2. These clear differences allow us to visualize the reason why bondi and mbondi2 suggested highly similar prediction results in all five GB methods.

$$\Delta G_{\text{solvation}} = \Delta G_{PB/GB} + \Delta G_{\text{nonpolar solvation energy}} \quad (2)$$

Comparison of Generalized Born Methods

From **Table 2**, we can clearly see that GB^{HCT} offered the best agreement with the experimental binding free energies (higher coefficient of determination) amongst the five GB methods using MD simulation trajectory data from 0.25 ns to 2 ns ($R^2 = 0.85 \sim 0.65$). However, if we used data from MD simulation trajectories longer than 2 ns, GB^{HCT} showed similar predictive performance compared to GB^{OBC}, GB^{OBC2}, and GB^{Neck2}. Moreover, because GB^{OBC} and GB^{OBC2} have a similar computational foundations, with only subtle differences in parameter settings, it is not surprising that GB^{OBC} and GB^{OBC2} resulted in similar predictive power for the FtFabI-benzimidazole system. With respect to the difference between GB^{Neck} and GB^{Neck2}, GB^{Neck2} outperformed GB^{Neck} as would be expected since GB^{Neck2} is an optimized version of GB^{Neck}, and includes a higher number of parameters and a broader range of scaling factors.[26]

On the other hand, GB^{Neck2} behaved differently compared to all of the other four GB methods, as summarized in **Figure 3** and **Supplementary Figure 2**. Even though the ΔG_{GB} and ΔG_{bind} terms calculated by GB^{HCT} converged throughout the 6 ns trajectories (2,400 frames) and GB^{Neck2} converged after 500 ps (200 frames), the ΔG_{GB} (the red line in **Figure 3a & 3b**) and ΔG_{bind} (the yellow line in **Figure 3a & 3b**) terms in GB^{Neck2} had consistently

greater fluctuation than with GB^{HCT} and the other GB methods **(Supplementary Figure 2)**. This was seen with all sixteen benzimidazole ligands (data not shown). **Figures 3c** and **3d** show the Q-Q plots for ΔG_{GB} using compound FabI 91, 6,000 ps (2,400 frames) using GB^{HCT} and GB^{neck2} methods, respectively. Compared to the nearly straight line in **Figure 3c** (GB^{HCT}), the two slightly rising tails in **Figure 3d** (GB^{Neck2}) suggest that the ΔG_{GB} population calculated by GB^{Neck2} may be skewed, which might bias the average ΔG_{GB} in GB^{Neck2}. A similar effect can be observed in the Q-Q plot for ΔG_{bind} calculated by GB^{HCT} and GB^{neck2}: the straighter line in **Figure 3e** (GB^{HCT}) suggests that ΔG_{bind} calculated by GB^{HCT} has a more normal distribution than that calculated using GB^{Neck2} (**Figure 3e**). Again, this may indicate that in calculations using GB^{Neck2}, ΔG_{GB}, $\Delta G_{solvation}$, and ΔG_{bind} might be slightly biased by the extreme values (outliers) and therefore provide less accurate prediction than the remaining four GB methods, at least using MD trajectories less than 3 ns.

Additionally, another reason why GB^{HCT}, GB^{OBC}, and GB^{OBC2} offered better agreement with experimental binding free energies than GB^{Neck1} and GB^{Neck2}, at least for this *Ft*FabI-benzimidazole system, is that the recently released GB^{Neck} and GB^{Neck2} methods have thus far only been optimized using peptide-protein systems, not protein-small molecule systems.[27] Future optimization of "neck region correction" GB methods covering non-peptide/non-protein systems will likely change this situation. As it stands, GB^{Neck1} and GB^{Neck2} are likely better suited than the GB^{HCT} GB^{OBC}, and GB^{OBC2} methods in predicting protein-protein binding free energies.

The Performance of QM/MM-GBSA

The Effect of Semi-Empirical QM Theory Levels on QM/MM-GBSA—The effects of three commonly used semi-empirical QM theory levels, Parameterized Model number 3 (PM3),[46,47] Austin Model 1 (AM1),[48] and Parameterized Model number 6 (PM6)[49] on QM/MM-GBSA are summarized in **Tables 3 - 5**. The PM3 Hamiltonian and QM-MM/GBSA together give the best agreement between experimental and predicted binding affinities, regardless of radii settings and GB methods **(Table 3)**. The AM1 Hamiltonian and QM-MM/GBSA together resulted in a slightly worse accuracy than the PM3 Hamiltonian for all conditions **(Table 4)**. Since the PM3 Hamiltonian is known to predict the intermolecular hydrogen bonds more accurately than the AM1 Hamiltonian,[50] the PM3 Hamiltonian would be a better choice than the AM1 Hamiltonian for the benzimidazole inhibitors, which forms key intermolecular hydrogen bonds with *Ft*FabI Tyr156 and the ribose on the nicotinamide ring of the cofactor NADH (Figure 4).[4,6]

The PM6 Hamiltonian is the recent advanced semi-empirical QM theory and it is believed to correct multiple defects in the AM1 and PM3 Hamiltonians.[49,51] However, use of the PM6 Hamiltonian in QM-MM/GBSA resulted in the worst binding affinity prediction of the three semi-empirical QM theory levels here **(Table 5)**. The PM6 Hamiltonian in QM-MM/GBSA using GB^{HCT}, GB^{OBC}, GB^{OBC2}, and GB^{Neck} radii sets resulted in no observed correlation between the predicted and experimental binding affinities **(Table 5)**. The PM6 Hamiltonian in QM-MM/GBSA using GB^{Neck2} was the only case where a moderate accuracy was observed. The ΔG_{bind}, ΔG_{GB}, and the QM/MM-GBSA electrostatic term (Self Consistent Energy, ΔG_{scf}) using the PM3 Hamiltonian are all converged **(Supplementary Figure 3)**,

similar to the AM1 and PM6 Hamiltonians (data not shown). A possible reason that the PM6 Hamiltonian performed poorly here is because in AMBER, the parameters of the PM6 Hamiltonian describing electrostatic interactions between QM and MM regions haven't been optimized and are borrowed from the PM3 Hamiltonian.[41] However, since the PM6 Hamiltonian is more advanced and covers broader cases than the PM3 Hamiltonian, the PM3 parameters might not be exclusive enough for the PM6 Hamiltonian. The missing parameters of the PM6 Hamiltonian are estimated, as detailed in the AMBER manual.[41] Therefore, the PM6 Hamiltonian requires more extensive tests, as pointed out in a previous study[34] and the AMBER user manual.[41] The future optimized PM6 parameters for electrostatic interactions between QM and MM regions are likely to significantly improve the PM6 Hamiltonian accuracy in the QM-MM/GBSA method within AMBER. Thus, since the PM3 Hamiltonian outperformed the AM1 and PM6 Hamiltonians in all conditions (MD simulation length, radii sets, etc.), only the PM3 Hamiltonian is considered in the following sections.

The Effect of MD Simulation Length on QM/MM-GBSA—The coefficient of determination between experimental and predicted binding free energies for different lengths of MD trajectories, various radii sets and semi-empirical QM methods in QM/MM-GBSA calculations, are summarized in **Tables 3 - 5**. It can be clearly seen that QM/MM-GBSA produced decreasing agreement with experimental binding free energies when longer MD trajectories were used with GB^{HCT}, GB^{OBC1}, GB^{OBC2}, and GB^{Neck1} in all the tested semi-empirical methods. However, the extent of decreasing predictive power with simulation time was significantly less in QM/MM-GBSA than that observed in MM-GBSA when using GB^{HCT}, GB^{OBC}, GB^{OBC2}, and GB^{Neck} with PM3 and AM1 semi-empirical methods **(Tables 2 - 4)**. This suggests that the extra QM and QM/MM terms in QM/MM-GBSA (**Equation 3 & 4**) may offset the amplification of "force field errors" and improve the predictive agreement with experimental binding free energies. With respect to GB^{Neck2} in QM/MM-GBSA using all the tested semi-empirical methods, surprisingly, the predictive power actually increased as the MD simulation lengths grew. The reason for this reversed trend compared to the other four GB methods can be traced back to the GB^{Neck2} results in MM-GBSA **(Table 2)**. Although the predictive power of GB^{Neck2} was seen to decrease with longer MD simulations, the extent of decrease was smaller than the other four GB methods. Moreover, the differences in behavior of GB^{Neck2} between MM-GBSA and QM/MM-GBSA can be further visualized in **Figures 3 & 5**. The Q-Q plot for ΔG_{GB} using GB^{neck2} suggests that ΔG_{GB} in MM-GBSA (**Figure 3d**) has more outliers than ΔG_{GB} in QM/MM-GBSA using the PM3 Hamiltonian (**Figure 5d**), which may bias the population mean and deteriorate the predictive results of the former. Similar results can be observed in the Q-Q plots of ΔG_{bind} using GB^{neck2} (**Figure 3f & 5f**). It seems that the GB^{Neck2} and extra QM energy terms in QM/MM-GBSA together provide a better description to ΔG_{GB} and ΔG_{bind} compared with the MM-GBSA results, and therefore offset the force field errors which could diminish the predictive power along the MD trajectory length.

$$E_{total}=E_{QM}+E_{MM}+E_{QM/MM}+G_{GB}+G_{nonpolar\ solvation\ energy} \quad (3)$$

$$G_{GB}=G_{polar}=G_{polor\ \ <QM>}+G_{polor\ \ <MM>}+G_{polor\ \ <QM-MM>} \quad (4)$$

The Effect of Radii Sets on QM/MM-GBSA—It has been previously noted by both AMBER and CHARMM developers that optimized radii specifically for QM Hamiltonians will advance the predictive power of QM/MM-GBSA methods.[35,52] With an understanding of their potential limitations, we investigated the optimized MM-GBSA radii sets (bondi, mbondi, and mbondi2) with QM/MM-GBSA methods in these studies. Interestingly, all three radii sets were able to provide satisfactory agreements with experimental data (R^2>0.70) using the five GB methods, various MD trajectory lengths, and the PM3 Hamiltonian, as discussed above and summarized in **Table 3**. Further, it can be clearly seen that the different radii settings yielded very similar results in both MM-GBSA **(Table 2)** and QM/MM-GBSA using the PM3 Hamiltonian **(Table 3)**. The reason behind these similarities is that MM-GBSA and QM/MM-GBSA are analogous. Also, even though QM/MM-GBSA includes extra QM and QM/MM energy terms, some of these energy terms such as $\Delta G_{polar<QM>}$ and $\Delta G_{polar<QM/MM>}$ (**Equation 3**) require radii sets as part of their ΔG_{polar} mathematical functions. Therefore, QM/MM-GBSA showed a predictive sensitivity similar to MM-GBSA in several specific situations. First, the mbondi radii set yielded similar coefficient of determination to bondi and mbondi2 when using GB^{HCT}. Second, the predictive power of bondi was always similar to mbondi2 in GB^{OBC}, GB^{OBC2}, GB^{Neck}, and GB^{Neck2} since bondi and mbondi2 are alike in nature (discussed above). The only difference between MM-GBSA and QM/MM-GBSA in terms of radii sets can be seen in **Table 3**. In both GB^{OBC1} and GB^{OBC2} methods, the mbondi radii set showed similar predictive power to bondi and mbondi2 radii sets with QM/MM-GBSA, whereas mbondi results were always inferior to bondi and mbondi2 with MM-GBSA. The reason for these different behaviors of GB^{OBC} and GB^{OBC2} in MM-GBSA and QM/MM-GBSA can be clearly visualized in **Supplementary Figure 2 & Supplementary Table 4** (MM-GBSA) and **Supplementary Figure 3 & Supplementary Table 5** (QM/MM-GBSA). While there is only one ΔG_{polar} term (MM ΔG_{polar} term) in MM-GBSA, QM/MM-GBSA includes extra QM and QM/MM ΔG_{polar} terms (**Equation 3**). Therefore, QM and QM/MM ΔG_{polar} terms together seemed to minimize the differences of the ΔG_{polar} term in the three tested radii sets, and the corresponding $\Delta G_{solvation}$. On the other hand, while the MM-GBSA electrostatic term in AMBER is radii independent, the QM/MM-GBSA electrostatic term (Self Consistent Energy, ΔG_{scf} in **Figure 5a,b**) is radii sensitive, as noted by Walker and Case.[35] Therefore, the QM/MM-GBSA electrostatic terms varied slightly among the three tested radii sets **(Figure 5 & Supplementary Table 5)**, while the MM-GBSA electrostatic terms were identical in the three tested radii sets. This also suggests that if one optimized radii sets for QM Hamiltonians, the QM/MM-GBSA should offer better descriptions, not only of $\Delta G_{solvation}$, but also of $\Delta G_{electrostatic}$.

Comparison of Generalized Born Methods on QM/MM-GBSA—With QM/MM-GBSA using the PM3 Hamiltonian **(Table 3)**, it can be seen that the GB^{OBC} method offered similar predictive power to GB^{OBC2}. This is likely because both GB methods share similar underlying principles with respect to their scaling functions to treat the radii sets.[24,25]

Likewise, while GB^{HCT} offered coefficient of determination similar to those of GB^{OBC} and GB^{OBC2} in all the MD simulation time frames, GB^{HCT} behaved differently to GB^{OBC} and GB^{OBC2} in MM-GBSA. This was quite surprising at first glance since the method to treat radii sets in GB^{HCT} is different from that of GB^{OBC} and GB^{OBC2}. One possible explanation for this behavior is that the extra QM and QM/MM ΔG_{polar} terms in QM/MM-GBSA are able to offset and minimize the differences between GB^{HCT}, GB^{OBC} and GB^{OBC2} in QM/MM-GBSA.[35] On the other hand, in QM/MM-GBSA using the PM3 Hamiltonian **(Table 3)**, the predictive power differences between the "neck correction" GB methods (GB^{Neck1} and GB^{Neck2}) and "non-neck correction" methods (GB^{HCT}, GB^{OBC1} and GB^{OBC2}) were significant. It is likely that the underlying theories behind the "neck correction" GB methods and "non-neck correction" methods are dissimilar to the extent that the extra QM and QM/MM ΔG_{polar} terms in QM/MM-GBSA were unable to offset the differences between "neck correction" GB methods and "non-neck correction" methods. Finally, in both MM-GBSA and QM/MM-GBSA using the PM3 Hamiltonian, GB^{Neck2} still outperformed GB^{Neck}, as GB^{Neck2} is the optimized version of the "neck correction" GB method.[27]

The Effect of Conformational Entropy

The effect of conformational entropy (48 frames) on MM-PBSA (2,400 frames) is summarized in **Table 6** and on MM-GBSA and QM/MM-GBSA (2,400 frames) in **Table 7**. The numerical values for conformational entropy and the corresponding absolute binding free energy of MM-PBSA, MM-GBSA and QM/MM-GBSA are summarized in **Supplementary Table 3, 4, & 5**, respectively. It can be seen that after including entropy, the predictive power (coefficient of determination) of MM/PBS and MM-GBSA decreased significantly, regardless of radii sets or GB methods **(Table 6 & 7)**. Interestingly, while the inclusion of entropy considerably reduced the predictive power of QM/MM-GBSA with GB^{Neck} and GB^{Neck2}, the negative effect of entropy inclusion on the predictive power of QM/MM-GBSA with GB^{HCT}, GB^{OBC} and GB^{OBC2} was less substantial **(Table 7)**. It appears that the conformational entropy compromised the predictive power in the *Ft*FabI-benzimidazole system due to large fluctuations.

Further analysis of the effect of conformational entropy on absolute binding free energy is summarized in **Figure 6**. **Figure 6a** shows that, although the cumulative average of conformational entropy (upper dashed red line) converged in the 48 frames entropy calculation, the instantaneous conformational entropy (upper solid black line) fluctuated greatly (± 10 kcal/mol) compared to the cumulative average. Such huge fluctuations suggest that a higher number of frames in entropy calculation are needed to improve the quality of entropy predictions and therefore yield more accurate absolute binding free energy, as suggested in a previous study.[21] Unfortunately, the high computational cost of entropy calculations prevented our further pursuit. For example, each *Ft*FabI-benzimizadole entropy calculation in 48 frames took 120-140 hours on TACC Lonestar's 48 large memory nodes, which is equivalent to 23,000-26,000 XSEDE Service Units per *Ft*FabI- benzimizadole set.

Because accurate absolute binding free energy calculations rely on simultaneous error cancellation between the entropy and enthalpy terms, enthalpy calculated from 2,400 frames

together with entropy calculated from 48 frames may not offer good quality absolute binding free energy predictions **(Table 6**, **column 3 & Table 7, column 4 & 10)**. To investigate this, we calculated the absolute binding free energy using 48 frames MM-PBSA and (QM/)MM-GBSA enthalpy and 48 frames entropy. The corresponding calculated absolute binding free energy was then correlated with the experimental binding free energy, as summarized in **Table 6, column 5 & Table 7, column 6 & 12.** The results showed that the enthalpy from 48 frames **(Table 6, column 4 & Table 7, column 5 & 11)** did not correlate well with the experimental data. This is most likely because the sample size of 48 frames was insufficient. The 48-frame enthalpy from MM-GBSA, the bondi radii setting and GB^{HCT} shown in the black histogram in **Figure 6b**, deviates significantly from the normal distribution seen for the 2,400-frame enthalpy histogram in **Figure 6c**. This suggests that the small sample size of 48 frames might offer a biased population mean. When the 48-frame enthalpy value was used with the 48-frame entropy value to calculate absolute binding free energy, the resulting value gave even worse agreement with the experimental binding free energy values (**Table 6, column 5 & Table 7, column 6 & 12**). This suggests that errors in entropy calculation using normal mode analysis here cannot be adequately cancelled using the enthalpy values from MM-PBSA and (QM/)MM-GBSA, even using the same MD frame samples for both calculations. Again, **Figure 6a** visualized the scenario here: Even though the instantaneous enthalpy from MM-GBSA (lower solid black line) was relatively stable, the "wild" instantaneous entropy (upper solid black line) still resulted in largely swinging and biased absolute free energy (blue dash line in **Figure 6a**) The histogram in **Figure 6b** visualized the distribution of 48 frames enthalpy from MM-GBSA (black), 48 frames entropy from normal mode analysis (red), and absolute free energy calculated from enthalpy minus entropy (blue). One can clearly see that entropy values in 48 frames distributed in a highly skewed shape with long double tails, which suggests the existence of extreme values. The extreme entropy values in some frames thus resulted in a skewed distribution with long double tails in absolute free binding energy (blue in **Figure 6b**). Thus, we will not include entropy calculation in future large scale benzimidazole prediction due to its high computational costs and relative inaccuracy.

Single MD Simulation Efficiency and Accuracy

MM-PBSA is about 60 times more computationally expensive (about 1 real world *hour* per 100 frames on TACC Lonestar using 48 CPU processors) than MM-GBSA and QM/MM-GBSA (about 1 real world *minute* per 100 frames on TACC Lonestar using 48 CPU processors). Therefore, MM-PBSA, together with bondi or mbondi2 settings using one 0.75-1 ns MD simulation trajectory (300-400 frames) can offer satisfactory predictive power (R^2= 0.82-0.83) with 3-4 hours of computation. Alternatively, MM-GBSA using bondi/mbondi2 settings with a 0.5-0.75 ns MD simulation trajectory (200-300 frames) is able to achieve R^2=0.85-0.88 with only 3-4 minutes of computation. Similarly, QM/MM-GBSA using GB^{HCT} and bondi/mbondi2 settings with 0.5 ns MD simulation trajectory (200 frames) can achieve R^2=0.81 with only 2 minutes of computation. This suggests that using one long MD simulation for large scale *Ft*FabI-benzimidazole predictions, MM-GBSA and QM/MM-GBSA will be more economical choices than MM-PBSA.

Multiple MD Simulation Efficiency and Accuracy

The MM-PBSA and (QM/)MM-GBSA results based on multiple independent trajectories together with various radii settings are summarized in **Table 8-10** accordingly. **Table 8-10** show that the differences between the length of MD simulations and different radii settings were not significant in all MM-PBSA and (QM/)MM-GBSA runs. Using multiple independent samplings, the differences between various GB methods in (QM-)MM-GBSA were also trivial. However, compared to one long MD simulation trajectory **(Tables 1-5)**, the predictive power using several short MD trajectories didn't decrease as it did when using longer MD simulation time frames **(Tables 8-10)**, suggesting that multiple independent samplings can offset force field errors.

Unlike using one long MD simulation, the predictive performance from multiple independent samplings was insensitive to various radii settings in all MM-PBSA and (QM/)MM-GBSA methods **(Table 8-10)**. In MM-PBSA **(Table 8)**, the three Born radii sets offered satisfactory predictive power ($R^2 > 0.7$) while the PARSE radii setting was slightly worse (R^2 in the 0.6 range). Using multiple independent samplings, the differences between (QM/)MM-GBSA were minimal. In (QM/)MM-GBSA together with multiple independent samplings **(Table 9 & 10)**, the three "non-neck" correction GB methods (GB^{HCT}, GB^{OBC}, GB^{OBC2}) behaved similarly but showed slight differences compared to the two neck correction GB methods (GB^{Neck} and GB^{Neck2}), which were similar to each other.

In terms of predictive power between the single, long MD simulation **(Table 1-5)** and multiple independent MD simulation **(Table 8-10)** methods, both provided similar predictive power using lower numbers of frames (600 and 1,200 frames). However, when larger numbers of frames were used, the predictive power decrease was negligible with the multiple independent simulation method but not with the single simulation. Taken together, these results suggest that methodology differences and errors may be minimized and averaged out using multiple independent samplings. With respect to computational efficiency, MM-PBSA is about 60-fold more computationally expensive than (QM/)MM-GBSA. Therefore, MM-GBSA together with GB^{HCT} using six 0.25 ns multiple independent MD simulations (600 frames) can offer very good agreement, $r^2 = 0.84$ **(Figure 7b)**, with experimental data after just 6 real world minutes of computation. Therefore, MM-GBSA and QM/MM-GBSA offer a better balance in terms of predictive power and computational efficiency than MM-PBSA with multiple independent samplings.

Conclusions

In this study, we have extensively compared three implicit solvent methods: MM-PBSA, MM-GBSA, and QM/MM-GBSA and the effects of radii sets, entropy, GB methods, QM Hamiltonians, sampling and simulation lengths using sixteen carefully chosen benzimidazole inhibitors of *F. tularensis* FabI. In the first part of the this study using one long MD simulation for each ligand (the traditional method), the various GB methods, QM Hamiltonians, and simulation lengths resulted in significantly different predictive power in MM-PBSA and (QM/)MM-GBSA results, while the effect of radii sets on prediction power is relatively milder. The QM/MM-GBSA method using GB^{Neck2}, mbondi2, and the PM3 Hamiltonian setting with 2,400 frames extracted evenly from single 6 ns MD simulations

offered the best agreement between predicted and experimental binding free energy (R^2 = 0.88, **Figure 7a**).

The inclusion of conformational entropy compromised the agreement between predicted absolute binding free energy and experimental binding free energy due to large fluctuations in the calculated entropy values. Theoretically, using a larger number of frames in the entropy calculations might increase its accuracy, but the associated high computational costs might not be easily affordable. Therefore, the implicit solvent free energy methods in this study (MM-PBSA and (QM/)MM-GBSA) were limited to comparing relative binding free energies of similar ligands due to the absence of accurate entropies. However, for the purposes of developing a rapid tool for energy predictions for a lead optimization program focusing on highly similar compounds, conformational entropy may be safely ignored as the implicit solvent methods used in this study can still be powerful tools in compound prioritization.

In the second part of the study, the prediction is based on the average of six 1 ns MD simulations for each FtFabI-benzimidazole system. We called this type of sampling, “multiple independent sampling” or “Monte Carlo like MD sampling”. In general, implicit solvent methods based on multiple independent samplings are less sensitive on radii sets, MD simulation length, and GB methods. This feature might minimize the future need of an entirely new validation study, when (1) a new scaffold of the same therapeutic target is pursued and (2) the same scaffold with additional moieties, which result in distinct physiochemical properties (charges, etc.) and binding modes from the previous validation sets, bring in different sensitivities on various parameters.

Because the predictive power of the multiple sampling method showed little decrease with MD simulation time, it can offer the same or better predictive power compared with the use of a single, long simulation with lower number of MD frames. For example, MM/GBSA together with GB^{HCT} and either bondi, mbondi or mbondi2, using 600 frames extracted evenly from six 0.25 ns MD simulations, can achieve a comparable agreement between predicted and experimental binding free energy (r^2 = 0.84, **Figure 7b**) to QM/MM-GBSA using GB^{Neck2}, mbondi2, and the PM3 Hamiltonian setting with 2,400 frames extracted evenly from 6 ns MD simulation (r^2 = 0.88, **Figure 7a**). Therefore, the multiple independent sampling method can be more computationally efficient than a single, long simulation method.

Different implicit solvents methods bring varied accuracy. In this study, MM-GBSA and QM/MM-GBSA brings better accuracy and higher efficiency than MM-PBSA, in either the multiple independent sampling method, or the tradition single, long simulation method **(Table 11a)**.

The effect of GB methods on accuracy **(Table 11b)** is more evident in the traditional one long simulation method. Unlike four other GB methods, GB^{Neck2} can offer the best accuracy in the 6 ns time frame, without a decrease in accuracy along the MD simulation length in both MM-GBSA and QM/MM-GBSA. GB^{HTC} could offer slightly better performance than GB^{OBC} and GB^{OBC2}. GB^{OBC} and GB^{OBC2} offer the comparable results, since they share

highly similar methodologies. Therefore, if the GB methods are applied on one MD trajectory for each ligand, the accuracy is GB^{Neck2} > GB^{HTC} >= GB^{OBC} = GB^{OBC2} > GB^{Neck}. However, the differences between GB methods are largely minimized in the multiple independent sampling.

The effect of radii sets on small molecule binding free energy prediction is relatively mild in the traditional long MD method, comparing to other parameters (**Table 11c**). In MM-PBSA, the performance is bondi = mbondi2 ≈ mbondi > PARSE. In MM/GBSA together with GB^{HCT},GB^{OBC}, GB^{Neck}, and GB^{Neck2}, the differences between radii sets are negligible. In MM/GBSA and GB^{OBC2}, the non-recommended mbondi setting shows inferior performance than recommended bondi and mbondi2 settings. Moreover, the effect of radii sets on QM/MM-GBSA is highly similar to MM-GBSA, besides in GB^{OBC2}, mbondi settings showed similar predictive power to bondi and mbondi2 with QM/MM-GBSA. On the other hand, the differences between radii sets are neutralized in the multiple sampling method.

QM Hamiltonians have a strong impact on QM/MM-GBSA results (**Table 11d**). In general, the performance is PM3 > AM1 > PM6. However, future optimized PM6 parameters may enhance the performance of the PM6 Hamiltonian in QM/MM-GBSA in AMBER.

To summarize, it is important, when optimizing computational protocols to predict binding free energy, to carefully investigate the optimal radii sets, entropy, sampling methods, GB methods, and QM Hamiltonians in (QM/)MM-P(G)BSA. Our results suggest that small deviations from optimized settings can have a significant impact on energy prediction results, not only for our *Ft*FabI-benzimidazole systems, but potentially other similar systems amenable to such lead optimization methods. Lastly, because MM/GBSA together with GB^{HCT}, mbondi, and 600 frames extracted evenly from six 0.25 ns MD simulations, provided accurate predictions efficiently, with less sensitivity on various parameters, this method will be applied to future large-scale lead optimizations of benzimidazole FabI inhibitors.

Supplementary Material

Refer to Web version on PubMed Central for supplementary material.

Acknowledgments

This work was supported in part by the National Institutes of Health Grant U01 AI077949. The computation resources were provided by the Texas Advanced Computing Center (TACC), Lonestar cluster at the University of Texas at Austin under the XSEDE Teragrid Grant TG-MCB090168. P.C.S was supported during part of this work by 13PRE-14800030, an American Heart Association pre-doctoral fellowship. K.E.H. was supported during a portion of this work by NIDCR 5T32-DE018381, UIC College of Dentistry, MOST Program. We thank the AMBER community, particularly Professors Adrian Roitberg, Carlos Simmerling, Ray Luo, Gerald Monard, Drs. Jason Swails, and Paul Gasper for AMBER technical support and helpful discussions.

Abbreviations

AM1	Austin Model 1
MD	Molecular Dynamics

MM-PBSA	Molecular Mechanics - Poisson-Boltzmann Surface Area
MM-GBSA	Molecular Mechanics - Generalized Born Surface Area
QM/MM-GBSA	Quantum Mechanics / Molecular Mechanics - Generalized Born Surface Area
FAS	Fatty Acid Synthesis
FtFabI	*Francisella tularensis* FabI
GAFF	general AMBER force field
PME	Particle Mesh Ewald
PM3	Parameterized Model number 3
PM6	Parameterized Model number 6
NMA	Normal Mode Analysis
RMSD	root-mean-square deviation
ΔG_{bind}	binding free energy
ΔH_{bind}	binding enthalpy
$\Delta G_{solvation}$	solvation free energy
ΔG_{GB}	Generalized Born polar free energy
ΔG_{PB}	Poisson-Boltzmann polar free energy

References and Notes

1. Christian MD. Crit Care Clin. 2013; 29(3):717–756. [PubMed: 23830660]
2. World Health Organization; Geneva, Switzerland: 2007.
3. Hevener KE, Mehboob S, Su PC, Truong K, Boci T, Deng J, Ghassemi M, Cook JL, Johnson ME. Journal of medicinal chemistry. 2012; 55(1):268–279. [PubMed: 22098466]
4. Mehboob S, Hevener KE, Truong K, Boci T, Santarsiero BD, Johnson ME. Journal of medicinal chemistry. 2012; 55(12):5933–5941. [PubMed: 22642319]
5. Lu H, England K, am Ende C, Truglio JJ, Luckner S, Reddy BG, Marlenee NL, Knudson SE, Knudson DL, Bowen RA, Kisker C, Slayden RA, Tonge PJ. ACS Chem Biol: United States. 2009:221–231.
6. Mehboob S, Song J, Hevener KE, Su P-C, Boci T, Brubaker L, Truong L, Mistry T, Deng J, Cook JL, Santarsiero BD, Ghosh AK, Johnson ME. Bioorganic & medicinal chemistry letters. 2015; 25(6):1292–1296. [PubMed: 25677657]
7. Zhang YY, Liu Y, Mehboob S, Song JH, Boci T, Johnson ME, Ghosh AK, Jeong H. Xenobiotica. 2013
8. Guimaraes CR, Cardozo M. J Chem Inf Model. 2008; 48(5):958–970. [PubMed: 18422307]
9. Homeyer N, Gohlke H. Journal of computational chemistry. 2013; 34(11):965–973. [PubMed: 23288722]
10. Zhu T, Lee H, Lei H, Jones C, Patel K, Johnson ME, Hevener KE. J Chem Inf Model. 2013; 53(3): 560–572. [PubMed: 23432621]
11. Rastelli G, Del Rio A, Degliesposti G, Sgobba M. J Comput Chem. 2010; 31(4):797–810. [PubMed: 19569205]
12. Pearlman DA. J Med Chem. 2005; 48(24):7796–7807. [PubMed: 16302819]

13. Steinbrecher T, Case DA, Labahn A. J Med Chem. 2006; 49(6):1837–1844. [PubMed: 16539369]
14. Wang J, Morin P, Wang W, Kollman PA. J Am Chem Soc. 2001; 123(22):5221–5230. [PubMed: 11457384]
15. Genheden S, Nilsson I, Ryde U. J Chem Inf Model. 2011; 51(4):947–958. [PubMed: 21417269]
16. Genheden S, Ryde U. J Chem Theory Comput. 2011; 7(11):3768–3778. [PubMed: 26598269]
17. Amaro RE, Cheng X, Ivanov I, Xu D, McCammon JA. Journal of the American Chemical Society. 2009; 131(13):4702–4709. [PubMed: 19296611]
18. Oehme DP, Brownlee RT, Wilson DJ. J Comput Chem. 2012; 33(32):2566–2580. [PubMed: 22915442]
19. Hou T, Wang J, Li Y, Wang W. J Chem Inf Model. 2011; 51(1):69–82. [PubMed: 21117705]
20. Genheden S. J Comput-Aided Mol Des. 2011; 25(11):1085–1093. [PubMed: 22101362]
21. Hou T, Wang J, Li Y, Wang W. Journal of chemical information and modeling. 2011; 51(1):69–82. [PubMed: 21117705]
22. Nina M, Beglov D, Roux B. The Journal of Physical Chemistry B. 1997; 101(26):5239–5248.
23. Hawkins GD, Cramer CJ, Truhlar DG. The Journal of Physical Chemistry. 1996; 100(51):19824–19839.
24. Onufriev A, Bashford D, Case DA. J Phys Chem B. 2000; 104(15):3712–3720.
25. Onufriev A, Bashford D, Case DA. Proteins. 2004; 55(2):383–394. [PubMed: 15048829]
26. Mongan J, Simmerling C, McCammon JA, Case DA, Onufriev A. J Chem Theory Comput. 2006; 3(1):156–169. [PubMed: 21072141]
27. Nguyen H, Roe DR, Simmerling C. Journal of chemical theory and computation. 2013; 9(4):2020–2034. [PubMed: 25788871]
28. Roe DR, Okur A, Wickstrom L, Hornak V, Simmerling C. J Phys Chem B. 2007; 111(7):1846–1857. [PubMed: 17256983]
29. Tan C, Tan Y-H, Luo R. J Phys Chem B. 2007; 111(42):12263–12274. [PubMed: 17918880]
30. Genheden S, Ryde U. J Comput Chem. 2010; 31(4):837–846. [PubMed: 19598265]
31. Seabra, G. d. M.; Walker, RC.; Elstner, M.; Case, DA.; Roitberg, AE. J Phys Chem A. 2007; 111(26):5655–5664. [PubMed: 17521173]
32. Park K, Götz AW, Walker RC, Paesani F. J Chem Theory Comput. 2012; 8(8):2868–2877. [PubMed: 26592126]
33. Cho AE, Guallar V, Berne BJ, Friesner R. J Comput Chem. 2005; 26(9):915–931. [PubMed: 15841474]
34. Götz AW, Clark MA, Walker RC. J Comput Chem. 2014; 35(2):95–108. [PubMed: 24122798]
35. Walker RC, Crowley MF, Case DA. Journal of computational chemistry. 2008; 29(7):1019–1031. [PubMed: 18072177]
36. Frisch, MJ.; Trucks, GW.; Schlegel, HB.; Scuseria, GE.; Robb, MA.; Cheeseman, JR.; Scalmani, G.; Barone, V.; Mennucci, B.; Petersson, GA.; Nakatsuji, H.; Caricato, M.; Li, X.; Hratchian, HP.; Izmaylov, AF.; Bloino, J.; Zheng, G.; Sonnenberg, JL.; Hada, M.; Ehara, M.; Toyota, K.; Fukuda, R.; Hasegawa, J.; Ishida, M.; Nakajima, T.; Honda, Y.; Kitao, O.; Nakai, H.; Vreven, T.; Montgomery, JA., Jr.; Peralta, JE.; Ogliaro, F.; Bearpark, M.; Heyd, JJ.; Brothers, E.; Kudin, KN.; Staroverov, VN.; Kobayashi, R.; Normand, J.; Raghavachari, K.; Rendell, A.; Burant, JC.; Iyengar, SS.; Tomasi, J.; Cossi, M.; Rega, N.; Millam, NJ.; Klene, M.; Knox, JE.; Cross, JB.; Bakken, V.; Adamo, C.; Jaramillo, J.; Gomperts, R.; Stratmann, RE.; Yazyev, O.; Austin, AJ.; Cammi, R.; Pomelli, C.; Ochterski, JW.; Martin, RL.; Morokuma, K.; Zakrzewski, VG.; Voth, GA.; Salvador, P.; Dannenberg, JJ.; Dapprich, S.; Daniels, AD.; Farkas, Ö.; Foresman, JB.; Ortiz, JV.; Cioslowski, J.; Fox, DJG. Inc.; Wallingford CT: 2009.
37. Bayly CI, P. C. Cornell W, Kollman PA. J. Phys. Chem. 1993:10269–10280.
38. Dupradeau FY, Pigache A, Zaffran T, Savineau C, Lelong R, Grivel N, Lelong D, Rosanski W, Cieplak P. Phys Chem Chem Phys. 2010; 12(28):7821–7839. [PubMed: 20574571]
39. Vanquelef E, Simon S, Marquant G, Garcia E, Klimerak G, Delepine JC, Cieplak P, Dupradeau FY. Nucleic Acids Res. 2011; 39(Web Server issue):W511–517. [PubMed: 21609950]

40. Wang J, Wolf RM, Caldwell JW, Kollman PA, Case DA. Journal of computational chemistry. 2004; 25(9):1157–1174. [PubMed: 15116359]

41. Case, DA.; T. A. D.; Cheatham, TE., III; Simmerling, CL.; Wang, J.; Duke, RE.; Luo, R.; Walker, RC.; Zhang, W.; Merz, KM.; Roberts, B.; Hayik, S.; Roitberg, A.; Seabra, G.; Swails, J.; Goetz, AW.; Kolossváry, I.; Wong, KF.; Paesani, F.; Vanicek, J.; Wolf, RM.; Liu, J.; Wu, X.; Brozell, SR.; Steinbrecher, T.; Gohlke, H.; Cai, Q.; Ye, X.; Wang, J.; Hsieh, M-J.; Cui, G.; Roe, DR.; Mathews, DH.; Seetin, MG.; Salomon-Ferrer, R.; Sagui, C.; Babin, V.; Luchko, T.; Gusarov, S.; Kovalenko, A.; Kollman, PA. University of California; San Francisco: 2012.

42. Miller BR, McGee TD, Swails JM, Homeyer N, Gohlke H, Roitberg AE. J Chem Theory Comput. 2012; 8(9):3314–3321. [PubMed: 26605738]

43. Sitkoff D, Sharp KA, Honig B. The Journal of Physical Chemistry. 1994; 98(7):1978–1988.

44. Pearlman DA, Case DA, Caldwell JW, Ross WS, Cheatham TE Iii, DeBolt S, Ferguson D, Seibel G, Kollman P. Computer Physics Communications. 1995; 91(1–3):1–41.

45. Nguyen H, Roe DR, Simmerling C. J Chem Theory Comput. 2013; 9(4):2020–2034. [PubMed: 25788871]

46. Stewart JJ. P. Journal of computational chemistry. 1989; 10(2):209–220.

47. Stewart JJP. Journal of computational chemistry. 1989; 10(2):221–264.

48. Dewar MJS, Zoebisch EG, Healy EF, Stewart JJP. Journal of the American Chemical Society. 1985; 107(13):3902–3909.

49. Stewart JP. J Mol Model. 2007; 13(12):1173–1213. [PubMed: 17828561]

50. Jurema MW, Shields GC. Journal of computational chemistry. 1993; 14(1):89–104.

51. Stewart JP. J Mol Model. 2009; 15(7):765–805. [PubMed: 19066990]

52. Pellegrini E, Field MJ. J Phys Chem A. 2002; 106(7):1316–1326.

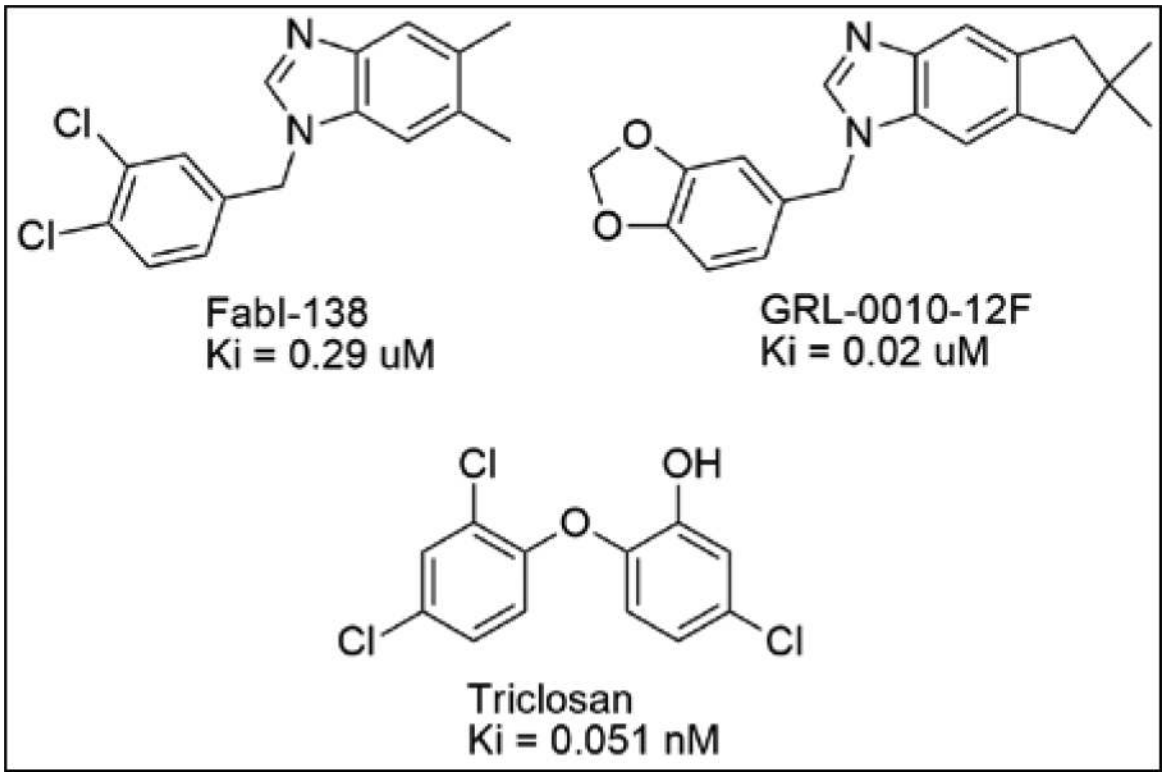

Figure 1.
Representative Benzimidazole FabI Inhibitors and Triclosan. [4-6]

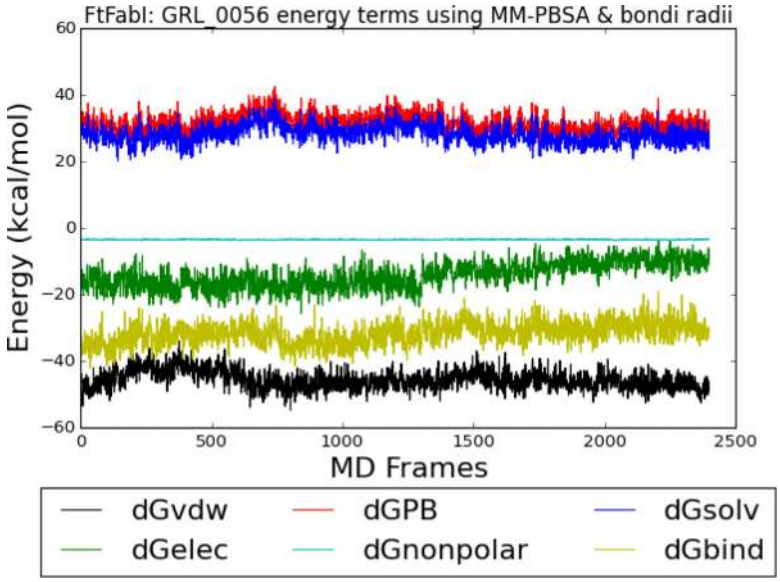

Figure 2.

FtFabI: GRL-0056 energy components using MM-PBSA and the bondi radii setting. Black, red, blue, green, cyan and yellow lines indicate the ΔG_{vdw}, $\Delta G_{GB,}$ $\Delta G_{solvation}$, $\Delta G_{electrostatic}$, $\Delta G_{nonpolar}$ and ΔG_{bind} terms respectively. The x axis is the frame number. Each frame is 2.5 ps. The total frame number is 2,400 frames, equal to 6 ns MD simulations.

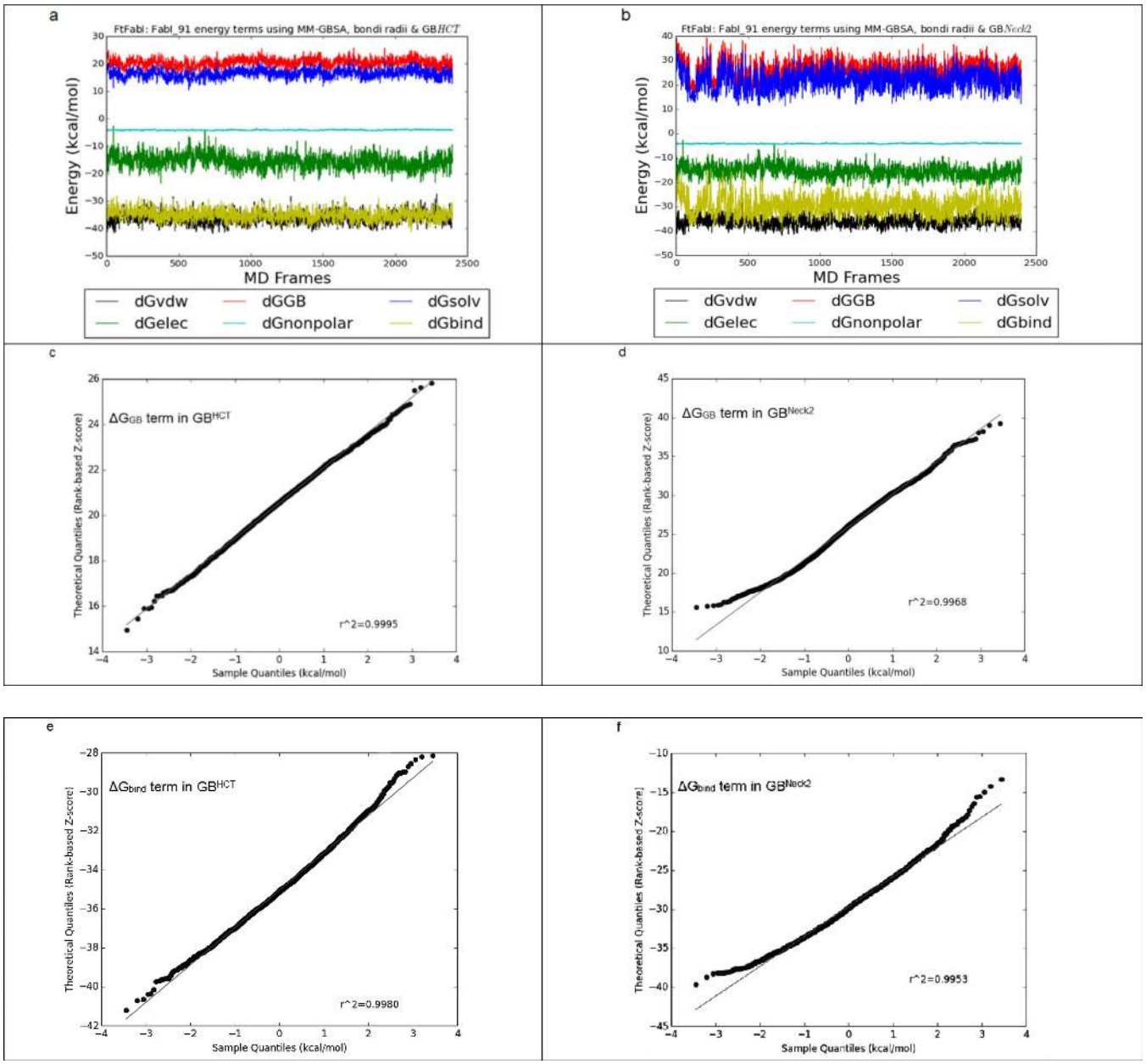

Figure 3.

A. FtFabI: FabI 91 energy components using MM-GBSA, bondi radii and GB^{HCT}. Black, red, blue, green, cyan and yellow lines indicate the ΔG_{vdw}, $\Delta G_{GB,}$ $\Delta G_{solvation}$, $\Delta G_{electrostatic}$, $\Delta G_{nonpolar}$ and ΔG_{bind} terms respectively. The x axis is the frame number. Each frame is 2.5 ps. The total frame number is 2,400 frames, equal to 6 ns MD simulations.

B. FtFabI: FabI 91 energy components using MM-GBSA, bondi radii and GB^{Neck2}.

C. The quantile-quantile plot (Q-Q plot) of the ΔG_{GB} term in GB^{HCT}.

D. The Q-Q plot of the ΔG_{GB} term in GB^{Neck2}.

E. The Q-Q plot of the ΔG_{bind} term in GB^{HCT}.

F. The Q-Q plot of the ΔG_{bind} term in GB^{Neck2}.

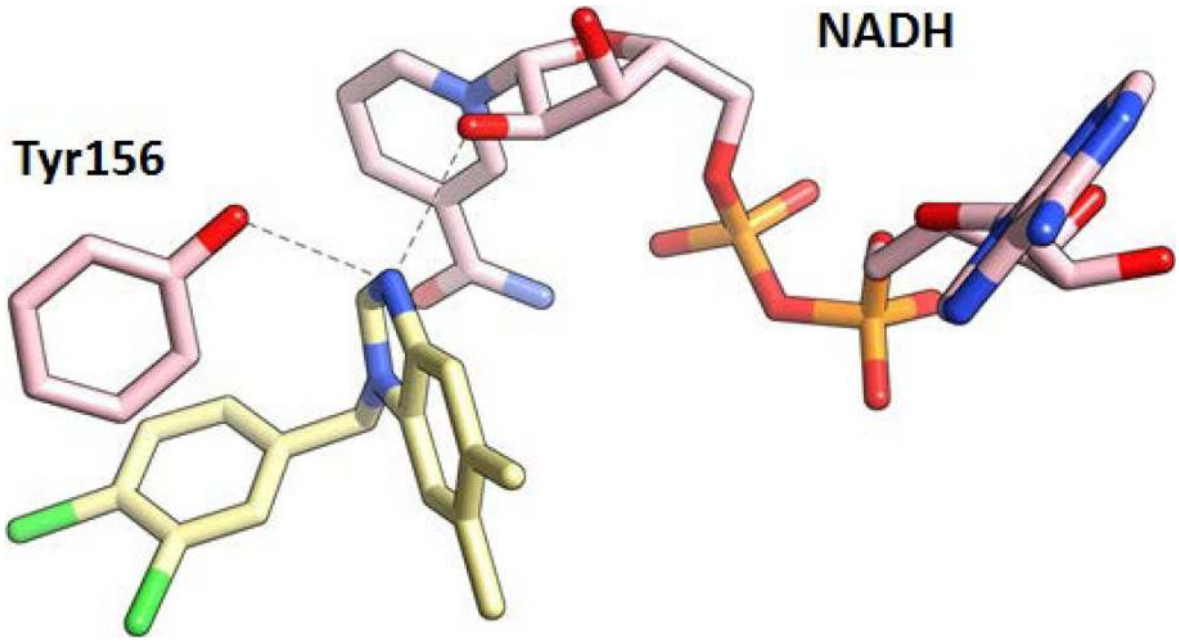

Figure 4.

The FabI 138 inhibitor (pdb code: 3UIC) and other benzimidazole inhibitors (pdb codes: 4J1N, 4J3F, 4J4T) form key intermolecular hydrogen bonds with the *Ft*FabI Tyr156 and the ribose on the nicotinamide ring of the cofactor NADH

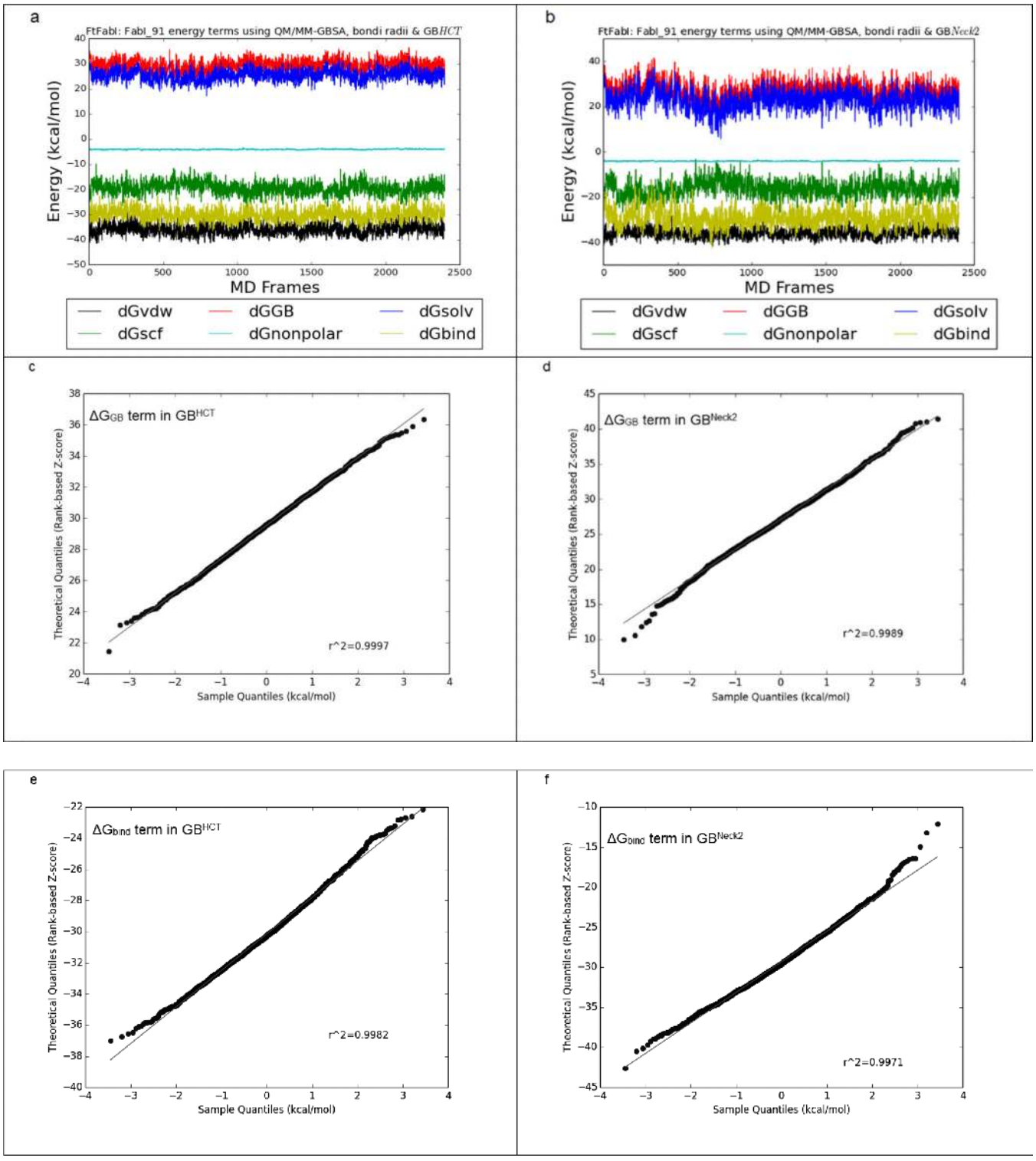

Figure 5.

A. FtFabI: FabI 91 energy components using QM/MM-GBSA, bondi radii and GB^{HCT}. Black, red, blue, green, cyan and yellow lines indicate the ΔG_{vdw}, ΔG_{GB}, $\Delta G_{solvation}$, ΔG_{SCF} (Self Consistent Energy), $\Delta G_{nonpolar}$ and ΔG_{bind} terms respectively. The x axis is the frame

number. Each frame is 2.5 ps. The total frame number is 2,400 frames, equal to 6 ns MD simulations.

B. FtFabI: FabI 91 energy components using QM/MM-GBSA, bondi radii and GB^{Neck2}. One can see from the ΔG_{GB} term (the red line) and the ΔG_{bind} term (the yellow line) in GB^{Neck2} fluctuates wilder than the one in GB^{HCT} (**Figure 5a**).

C. The quantile-quantile plot (Q-Q plot) of the ΔG_{GB} term in GB^{HCT}.

D. The Q-Q plot of the ΔG_{GB} term in GB^{Neck2}.

E. The Q-Q plot of the ΔG_{bind} term in GB^{HCT}.

F. The Q-Q plot of the ΔG_{bind} term in GB^{Neck2}.

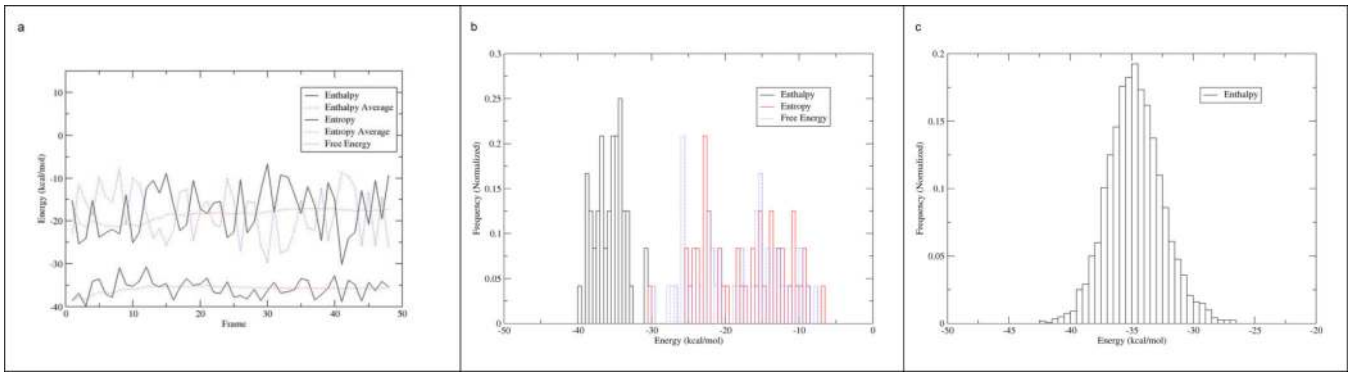

Figure 6.

A. The enthalpy, entropy and binding free energy components (48 frames) in the 6 ns MD simulation of FtFabI: FabI-135 using MM/GBSA, the bondi radii setting and GB^{HCT}. The upper solid black and dash red line represents instanenous and cumulative average entropy respectively and the lower solid black and dash red line represents instanenous and cumulative average enthalpy. The blue line represents binding free energy.

B. The histogram view of the enthalpy, entropy and binding free energy (48 frames) in the 6 ns MD simulation of FtFabI: FabI-135 using MM/GBSA, the bondi radii setting and GB^{HCT}.

C. The histogram view of the enthalpy (2,400 frames) in the 6 ns MD simulation of FtFabI: FabI-135 using MM/GBSA, the bondi radii setting and GB^{HCT}.

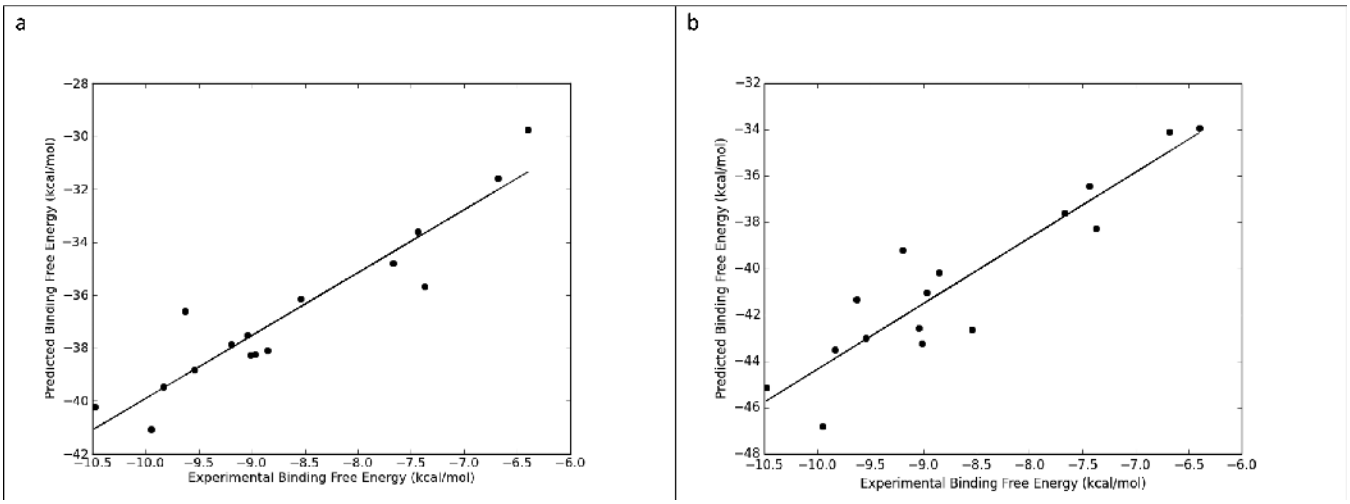

Figure 7.

A. The correlation plot between experimental and predicited binding free energy using QM-MM/GBSA, GB^{Neck2}, mbondi2 & 2,400 frames evenly extracted from 6 ns long MD simulation trajectories ($R^2 = 0.88$).

B. The correlation plot between experimental and predicited binding free energy using MM/GBSA, GB^{HCT}, mbondi & 600 frames evenly extracted from six 0.25 ns long MD simulation trajectories ($R^2 = 0.84$).

Table 1

The coefficient of determination of Experimental and Predicted Binding Free Energies of Different MD Trajectory Lengths and Radii Sets in MM/PBSA Calculations.[a]

Radii Sets	$R^2_{0.25ns}$	$R^2_{0.5ns}$	$R^2_{0.75ns}$	R^2_{1ns}	R^2_{2ns}	R^2_{3ns}	R^2_{4ns}	R^2_{5ns}	R^2_{6ns}
bondi	0.78	0.82	0.83	0.82	0.74	0.61	0.49	0.4	0.36
mbondi	0.71	0.75	0.76	0.77	0.72	0.62	0.54	0.48	0.45
mbondi2	0.79	0.82	0.83	0.82	0.74	0.61	0.49	0.43	0.37
PARSE	0.62	0.67	0.72	0.75	0.77	0.68	0.61	0.53	0.48

[a] R^2_n: "R^2" stands for coefficient of determination in the MM/PBSA calculation. Here 100, 400, 1200, 2400 MD simulation frames were evenly extracted from one 0.25, 1, 3, 6 ns MD simulation trajectories, respectively.

J Comput Chem. Author manuscript; available in PMC 2016 September 30.

Table 2

The coefficient of determination of Experimental and Predicted Binding Free Energies of Different MD Trajectory Lengths and Radii Sets in MM/GBSA Calculations.[a]

Radii Sets	GB	$R^2_{0.25ns}$ [a]	$R^2_{0.5ns}$	$R^2_{0.75ns}$	R^2_{1ns}	R^2_{2ns}	R^2_{3ns}	R^2_{4ns}	R^2_{5ns}	R^2_{6ns}
bondi	GB^{HCT}	0.85	0.88	0.85	0.81	0.65	0.53	0.45	0.41	0.41
mbondi	GB^{HCT}	0.81	0.83	0.8	0.75	0.59	0.51	0.45	0.43	0.44
mbondi2	GB^{HCT}	0.85	0.87	0.85	0.8	0.64	0.52	0.44	0.4	0.41
bondi	GB^{OBC}	0.79	0.83	0.82	0.78	0.63	0.51	0.42	0.37	0.38
mbondi	GB^{OBC}	0.68	0.71	0.7	0.67	0.52	0.43	0.37	0.35	0.36
mbondi2	GB^{OBC}	0.77	0.81	0.8	0.77	0.61	0.48	0.4	0.36	0.36
bondi	GB^{OBC2}	0.77	0.82	0.81	0.77	0.62	0.49	0.4	0.35	0.36
mbondi	GB^{OBC2}	0.59	0.64	0.62	0.59	0.42	0.31	0.25	0.23	0.24
mbondi2	GB^{OBC2}	0.73	0.78	0.77	0.74	0.57	0.44	0.35	0.31	0.32
bondi	GB^{Neck}	0.57	0.58	0.57	0.56	0.4	0.26	0.18	0.15	0.16
mbondi2	GB^{Neck}	0.52	0.53	0.53	0.52	0.36	0.23	0.16	0.13	0.15
bondi	GB^{Neck2}	0.63	0.68	0.6	0.6	0.52	0.5	0.49	0.48	0.5
mbondi2	GB^{Neck2}	0.63	0.67	0.6	0.6	0.51	0.5	0.5	0.49	0.51

[a] R^2_n: "R^2" stands for coefficient of determination in the MM/GBSA calculation. Here 100, 400, 1200, 2400 MD simulation frames were evenly extracted from one 0.25, 1, 3, 6 ns MD simulation trajectories, respectively.

Table 3

The coefficient of determination of Experimental and Predicted Binding Free Energies of Different MD Trajectory Lengths and Radii Sets in QM-MM/GBSA Calculations using the PM3 Hamiltonian.[a]

Radii Sets	GB	$R^2_{0.25ns}$ [a]	$R^2_{0.5ns}$	$R^2_{0.75ns}$	R^2_{1ns}	R^2_{2ns}	R^2_{3ns}	R^2_{4ns}	R^2_{5ns}	R^2_{6ns}
bondi	GB^{HCT}	0.78	0.81	0.78	0.73	0.64	0.58	0.53	0.52	0.54
mbondi	GB^{HCT}	0.76	0.79	0.75	0.69	0.59	0.56	0.54	0.55	0.57
mbondi2	GB^{HCT}	0.78	0.81	0.78	0.73	0.64	0.58	0.54	0.52	0.54
bondi	GB^{OBC}	0.76	0.79	0.76	0.72	0.64	0.6	0.56	0.54	0.56
mbondi	GB^{OBC}	0.72	0.75	0.71	0.67	0.57	0.55	0.53	0.54	0.56
mbondi2	GB^{OBC}	0.76	0.79	0.76	0.71	0.63	0.59	0.55	0.53	0.55
bondi	GB^{OBC2}	0.75	0.79	0.75	0.71	0.62	0.56	0.51	0.49	0.51
mbondi	GB^{OBC2}	0.72	0.75	0.71	0.64	0.51	0.47	0.44	0.44	0.46
mbondi2	GB^{OBC2}	0.75	0.78	0.75	0.69	0.59	0.54	0.49	0.47	0.49
bondi	GB^{Neck}	0.73	0.73	0.69	0.64	0.52	0.46	0.4	0.39	0.42
mbondi2	GB^{Neck}	0.72	0.72	0.68	0.63	0.51	0.44	0.38	0.37	0.4
bondi	GB^{Neck2}	0.62	0.66	0.62	0.65	0.69	0.76	0.79	0.82	0.86
mbondi2	GB^{Neck2}	0.64	0.67	0.64	0.67	0.7	0.78	0.81	0.83	0.88

[a] R^2_n: "R^2" stands for coefficient of determination in the QM-MM/GBSA calculation. Here 100, 400, 1200, 2400 MD simulation frames were evenly extracted from one 0.25, 1, 3, 6 ns MD simulation trajectories, respectively.

Table 4

The coefficient of determination of Experimental and Predicted Binding Free Energies of Different MD Trajectory Lengths and Radii Sets in QM-MM/GBSA Calculations using the AM1 Hamiltonian.[a]

Radii Sets	GB	$R^2_{0.25ns}$ [a]	$R^2_{0.5ns}$	$R^2_{0.75ns}$	R^2_{1ns}	R^2_{2ns}	R^2_{3ns}	R^2_{4ns}	R^2_{5ns}	R^2_{6ns}
bondi	GB^{HCT}	0.78	0.83	0.79	0.74	0.64	0.55	0.47	0.44	0.45
mbondi	GB^{HCT}	0.74	0.78	0.73	0.69	0.58	0.53	0.49	0.48	0.50
mbondi2	GB^{HCT}	0.79	0.83	0.79	0.74	0.64	0.56	0.48	0.44	0.46
bondi	GB^{OBC}	0.67	0.75	0.72	0.69	0.60	0.54	0.45	0.41	0.42
mbondi	GB^{OBC}	0.60	0.67	0.63	0.60	0.51	0.48	0.43	0.42	0.44
mbondi2	GB^{OBC}	0.68	0.75	0.72	0.69	0.59	0.53	0.45	0.41	0.42
bondi	GB^{OBC2}	0.65	0.74	0.72	0.68	0.57	0.50	0.41	0.37	0.37
mbondi	GB^{OBC2}	0.61	0.68	0.64	0.58	0.46	0.40	0.34	0.33	0.35
mbondi2	GB^{OBC2}	0.66	0.74	0.71	0.66	0.55	0.47	0.39	0.35	0.36
bondi	GB^{Neck}	0.62	0.63	0.58	0.53	0.40	0.31	0.24	0.22	0.24
mbondi2	GB^{Neck}	0.62	0.63	0.58	0.53	0.40	0.31	0.24	0.22	0.24
bondi	GB^{Neck2}	0.55	0.61	0.60	0.62	0.64	0.69	0.70	0.74	0.79
mbondi2	GB^{Neck2}	0.57	0.63	0.62	0.65	0.67	0.72	0.73	0.76	0.81

[a] R^2_n: "R^2" stands for coefficient of determination in the QM-MM/GBSA calculation. Here 100, 400, 1200, 2400 MD simulation frames were evenly extracted from one 0.25, 1, 3, 6 ns MD simulation trajectories, respectively.

Table 5

The coefficient of determination of Experimental and Predicted Binding Free Energies of Different MD Trajectory Lengths and Radii Sets in QM-MM/GBSA Calculations using the PM6 Hamiltonian.[a]

Radii Sets	GB	$R^2_{0.25ns}$ [a]	$R^2_{0.5ns}$	$R^2_{0.75ns}$	R^2_{1ns}	R^2_{2ns}	R^2_{3ns}	R^2_{4ns}	R^2_{5ns}	R^2_{6ns}
bondi	GB^{HCT}	0.54	0.61	0.57	0.52	0.41	0.28	0.18	0.14	0.14
mbondi	GB^{HCT}	0.49	0.55	0.51	0.46	0.36	0.30	0.26	0.25	0.27
mbondi2	GB^{HCT}	0.56	0.63	0.59	0.54	0.43	0.30	0.20	0.16	0.17
bondi	GB^{OBC}	0.15	0.21	0.20	0.17	0.09	0.04	0.01	0.01	0.01
mbondi	GB^{OBC}	0.13	0.18	0.16	0.13	0.07	0.05	0.04	0.03	0.04
mbondi2	GB^{OBC}	0.17	0.24	0.22	0.19	0.11	0.06	0.02	0.01	0.02
bondi	GB^{OBC2}	0.16	0.23	0.22	0.19	0.11	0.05	0.02	0.01	0.01
mbondi	GB^{OBC2}	0.12	0.17	0.15	0.11	0.05	0.02	0.01	0.01	0.02
mbondi2	GB^{OBC2}	0.17	0.24	0.23	0.19	0.11	0.05	0.02	0.01	0.02
bondi	GB^{Neck}	0.24	0.26	0.23	0.20	0.13	0.07	0.03	0.02	0.03
mbondi2	GB^{Neck}	0.26	0.29	0.26	0.23	0.15	0.09	0.05	0.04	0.05
bondi	GB^{Neck2}	0.52	0.57	0.55	0.56	0.56	0.57	0.57	0.60	0.64
mbondi2	GB^{Neck2}	0.53	0.57	0.54	0.56	0.56	0.57	0.58	0.60	0.64

[a] R^2_n: "R^2" stands for coefficient of determination in the QM-MM/GBSA calculation. Here 100, 400, 1200, 2400 MD simulation frames were evenly extracted from one 0.25, 1, 3, 6 ns MD simulation trajectories, respectively.

Table 6

Summary of the Impact of Entropy on Predicted Binding Free Energies of MD Trajectories of Different Lengths and Radii Sets in MM/PBSA Calculations.

1	2	3	4	5
Radii Sets	$\mathbf{R^2_{6ns}}$ *a,b*	$\mathbf{R^2_{6ns}}$ *c*	$\mathbf{R^2_{6ns}}$ *d*	$\mathbf{R^2_{6ns}}$ *e*
bondi	0.36	0.06	0.21	0
mbondi	0.45	0.12	0.29	0
mbondi2	0.37	0.06	0.22	0
PARSE	0.48	0.15	0.27	0.01

a R^2_n: "R^2" stands for coefficient of determination in the MM/PBSA calculation. Here 2,400 MD simulation frames were evenly extracted from 6 ns MD simulation trajectories.

b 2,400 frames calculated enthalpy & no calculated entropy

c 2,400 frames calculated enthalpy & 48 frames calculated entropy

d 48 frames calculated enthalpy & no calculated entropy

e 48 frames calculated enthalpy & 48 frames calculated entropy

Table 7

Summary of Impact of Entropy on Predicted Binding Free Energies of MD Trajectories of Different Lengths and Radii Sets in MM/GBSA and QM-MM/GBSA Calculations

MM/GBSA						QM-MM/GBSA					
1	2	3	4	5	6	7	8	9	10	11	12
Radii Sets	GB	R^2_{6ns} [a,b]	R^2_{6ns} [c]	R^2_{6ns} [d]	R^2_{6ns} [e]	Radii Sets	GB	R^2_{6ns} [a,b]	R^2_{6ns} [c]	R^2_{6ns} [d]	R^2_{6ns} [e]
bondi	GB^{HCT}	0.41	0.24	0.37	0.14	bondi	GB^{HCT}	0.54	0.52	0.54	0.48
mbondi	GB^{HCT}	0.44	0.3	0.42	0.22	mbondi	GB^{HCT}	0.57	0.59	0.59	0.58
mbondi2	GB^{HCT}	0.41	0.24	0.37	0.14	mbondi2	GB^{HCT}	0.54	0.54	0.54	0.50
bondi	GB^{OBC}	0.38	0.12	0.31	0.04	bondi	GB^{OBC}	0.56	0.51	0.56	0.41
mbondi	GB^{OBC}	0.36	0.12	0.30	0.04	mbondi	GB^{OBC}	0.56	0.54	0.57	0.49
mbondi2	GB^{OBC}	0.36	0.12	0.29	0.03	mbondi2	GB^{OBC}	0.55	0.52	0.55	0.43
bondi	GB^{OBC2}	0.36	0.13	0.27	0.04	bondi	GB^{OBC2}	0.51	0.45	0.49	0.36
mbondi	GB^{OBC2}	0.24	0.05	0.16	0.00	mbondi	GB^{OBC2}	0.46	0.42	0.43	0.35
mbondi2	GB^{OBC2}	0.32	0.1	0.23	0.02	mbondi2	GB^{OBC2}	0.49	0.45	0.46	0.35
bondi	GB^{Neck}	0.16	0.00	0.07	0.02	bondi	GB^{Neck}	0.42	0.28	0.35	0.14
mbondi2	GB^{Neck}	0.15	0.00	0.06	0.02	mbondi2	GB^{Neck}	0.4	0.28	0.34	0.15
bondi	GB^{Neck2}	0.5	0.07	0.42	0.06	bondi	GB^{Neck2}	0.86	0.47	0.75	0.42
mbondi2	GB^{Neck2}	0.51	0.07	0.43	0.07	mbondi2	GB^{Neck2}	0.88	0.52	0.76	0.46

[a] R^2_n: "R^2" stands for coefficient of determination in the MM/PBSA calculation. Here 2,400 MD simulation frames were evenly extracted from 6 ns MD simulation trajectories.

[b] 2,400 frames calculated enthalpy & no calculated entropy

[c] 2,400 frames calculated enthalpy & 48 frames calculated entropy

[d] 48 frames calculated enthalpy & no calculated entropy

[e] 48 frames calculated enthalpy & 48 frames calculated entropy

Table 8

The coefficient of determination of Experimental and Predicted Binding Free Energies of Different Multiple MD Trajectory Lengths and Radii Sets in MM/PBSA Calculations.

Radii Sets	$R^2_{0.25n}$	$R^2_{0.5ns}$	$R^2_{0.75}$	R^2_{1ns}
bondi	0.77	0.73	0.73	0.75
mbondi	0.76	0.74	0.74	0.76
mbondi2	0.77	0.73	0.73	0.76
PARSE	0.6	0.59	0.61	0.65

[a] R^2_n: "R^2" stands for coefficient of determination in the MM/PBSA calculation. Here 600, 1200, 1800, 2400 MD simulation frames were evenly extracted from six 0.25, 0.5, 0.75, 1 ns MD simulation trajectories, respectively.

Table 9

The coefficient of determination of Experimental and Predicted Binding Free Energies of Different Multiple MD Trajectory Lengths and Radii Sets in MM/GBSA Calculations.[a]

Radii Sets	GB	$R^2_{0.25ns}$ [a]	$R^2_{0.5ns}$	$R^2_{0.75ns}$	R^2_{1ns}
bondi	GB^{HCT}	0.84	0.83	0.82	0.82
mbondi	GB^{HCT}	0.84	0.84	0.83	0.82
mbondi2	GB^{HCT}	0.84	0.83	0.82	0.82
bondi	GB^{OBC}	0.81	0.8	0.8	0.8
mbondi	GB^{OBC}	0.81	0.8	0.8	0.8
mbondi2	GB^{OBC}	0.81	0.8	0.8	0.8
bondi	GB^{OBC2}	0.81	0.79	0.79	0.79
mbondi	GB^{OBC2}	0.78	0.77	0.76	0.76
mbondi2	GB^{OBC2}	0.8	0.78	0.79	0.78
bondi	GB^{Neck}	0.73	0.7	0.71	0.71
mbondi2	GB^{Neck}	0.72	0.69	0.7	0.7
bondi	GB^{Neck2}	0.72	0.68	0.68	0.66
mbondi2	GB^{Neck2}	0.72	0.69	0.68	0.66

[a] R^2_n: "R^2" stands for coefficient of determination in the MM/GBSA calculation. Here 600, 1200, 1800, 2400 MD simulation frames were evenly extracted from six 0.25, 0.5, 0.75, 1 ns MD simulation trajectories, respectively.

Table 10

The coefficient of determination of Experimental and Predicted Binding Free Energies of Multiple MD of Different Trajectory Lengths and Radii Sets in QM-MM/GBSA Calculations.[a]

Radii	GB	$R^2_{0.25ns}$ [a]	$R^2_{0.5ns}$	$R^2_{0.75ns}$	R^2_{1ns}
bondi	GB^{HCT}	0.76	0.75	0.75	0.75
mbondi	GB^{HCT}	0.76	0.75	0.76	0.75
mbondi2	GB^{HCT}	0.76	0.75	0.75	0.75
bondi	GB^{OBC}	0.73	0.72	0.72	0.72
mbondi	GB^{OBC}	0.73	0.73	0.73	0.72
mbondi2	GB^{OBC}	0.73	0.72	0.72	0.72
bondi	GB^{OBC2}	0.73	0.72	0.72	0.72
mbondi	GB^{OBC2}	0.73	0.73	0.73	0.72
mbondi2	GB^{OBC2}	0.73	0.72	0.72	0.71
bondi	GB^{Neck}	0.68	0.67	0.67	0.67
mbondi2	GB^{Neck}	0.68	0.67	0.67	0.66
bondi	GB^{Neck2}	0.71	0.69	0.7	0.69
mbondi2	GB^{Neck2}	0.71	0.7	0.71	0.7

[a] R^2_n: "R^2" stands for coefficient of determination in the QM-MM/GBSA calculation. Here 600, 1200, 1800, 2400 MD simulation frames were evenly extracted from six 0.25, 0.5, 0.75, 1 ns MD simulation trajectories, respectively.

Table 11

Summary of the Effect of Parameters on Predictive Power

		Traditional method	**Multiple Independent Sampling**
a. Accuracy of Implicit Solvent Methods		QM/MM-GBSA > MM-GBSA > MM-PBSA	QM/MM-GBSA ≈ MM-GBSA > MM-PBSA
		MM-GBSA & QM/MM-GBSA	
		Traditional method	Multiple Independent Sampling
b. Accuracy of GB Methods		GB^{Neck2} > GB^{HTC} >= GB^{OBC} = GB^{OBC2} > GB^{Neck}	Differences are minimized
		MM-PBSA	
		Traditional method	Multiple Independent Sampling
c. Accuracy of Radii Settings		bondi = mbondi2 ≈ mbondi > PARSE	Differences are minimized
		MM-GBSA & QM/MM-GBSA	
GB Method Names	AMBER igb flag	Traditional method	Multiple Independent Sampling
GB^{HCT}	1	bondi = mbondi2 ≈ mbondi[a]	Differences are minimized
GB^{OBC}	2	bondi[a] = mbondi2[a] ≈ mbondi	Differences are minimized
GB^{OBC2}	5	bondi[a] = mbondi2[a] >≈[b] mbondi	Differences are minimized
GB^{Neck}	7	mbondi2[a,c] ≈ bondi	Differences are minimized
GB^{Neck2}	8	mbondi2[a,d] ≈ bondi	Differences are minimized
		QM/MM-GBSA	
d. Accuracy of PM Hamiltonians		PM3 > AM1 > PM6	

[a] AMBER user manual recommended radii sets for the GB methods.

[b] In MM-GBSA and GB^{OBC2}: bondi[a] = mbondi2[a] > mbondi. In QM/MM-GBSA and GB^{OBC2}: bondi[a] = mbondi2[a] ≈ mbondi

[c] bondi might also work, but it might cause instability in the native peptide REMD type of simulation.

[d] mbondi3 is recommended in the MD/REMD type of simulation.